A Scanning Radiation Thermometry Technique for Determining Temperature Distribution in Gas Turbines

M. De Lucia

G. Masotti
Research Fellow.

Department of Energy Engineering,
Università di Firenze,
Florence, Italy

A scanning radiation thermometry technique for determining temperature distributions in gas turbines is presented. The system, an enhancement of an earlier work, can be used by operators even without special training, since the temperature distribution is measured and corrected in terms of the error due to the reflected radiation only on the basis of the turbine's known geometry and the physical properties of the materials. In the proposed model, the surface-exitent radiances are directly acquired via 360-deg scans. Experimental testing was performed on a static turbine-blading model. Since the angle factors emerged as a notable influence on the accuracy of the model, two angle factor calculation methods, selected for suitability from a literature survey, are exhaustively investigated, and their selection criteria defined.

Introduction

In gas turbines, temperature distribution must be known throughout the life of the machine if performance is to be properly monitored. Yet, owing to the inherent difficulties and expense involved in determining it, this information is not always readily available, even to machine operators. With noncontact radiation thermometers, temperatures can be measured in the harshest environments, especially when moving components are involved. In an earlier paper, De Lucia and Lanfranchi (1994) proposed a radiation thermometry model based on the use of theoretical temperature distributions to correct target temperature. This work presents an enhanced version of the earlier system that enables the determination of temperature distribution on the basis of multiple radiation thermometer measurements.

In a radiation thermometry system, the radiation emitted by each turbine component is measured and its temperature determined with the aid of calculation assumptions (Beynon, 1981, 1982; Scotto and Eismeier, 1980). Provided there is optical access, temperatures may be rapidly and accurately measured at any point or profile of the rotating component (Douglas, 1980; Kirby et al., 1986). However, in nonisothermal systems such as gas turbine cooled stages, the total sensed (exitent) radiation comprises two major components (DeWitt and Incropera, 1988):

1 Radiation produced as the result of the target surface temperature (emittent radiation)
2 Radiation reflected due to interreflection between the target surface and its surroundings.

Consequently, we must first estimate and subtract from the exitent radiations (L_{ex}) the reflected radiation (L_r), which is related to the surface temperature distribution and geometry, before proceeding to invert Planck's law. Hence, since the radiation thermometer reads the global target radiation, the reflected component represents a bothersome source of error. In the earlier model, the temperature distribution and geometry are separate, thereby allowing correction of the measured value with good approximation. However, the earlier model requires input of the theoretical temperature distribution, which, in many cases, is unknown to those actually carrying out the measurements. As a result, despite its simplicity and ease of use, it is not always suitably accurate, especially when the machine behavior deviates from theoretical predictions. This limitation has been overcome in the present model, which has the advantage of not requiring prior knowledge of the theoretical temperature distribution to determine gas turbine temperatures accurately.

Description of the Model

Like its predecessor, the present model considers surface-exitent thermal radiations in calculating the temperature distribution, with the difference that the radiations are measured by a scanning radiation thermometry technique solely on the basis of the known geometry and the physical properties of the materials. In the scanning radiation thermometry

Contributed by the International Gas Turbine Institute and presented at the 39th International Gas Turbine and Aeroengine Congress and Exposition, The Hague, The Netherlands, June 13–16, 1994. Manuscript received by the International Gas Turbine Institute February 4, 1994. Paper No. 94-GT-39. Associate Technical Editor: E. M. Greitzer.

technique, all the radiations exiting the surfaces that can be optically accessed by a 360-deg radiation thermometer scan are acquired and used in calculating the radiations exchanged by the surfaces through their angle factors.

The following assumptions were made:

- Radiative heat transfer was assumed at steady-state conditions.
- All radiances, powers, energies, and emissivities were assumed spectral, allowing evaluation at the radiant thermometer's constant wavelength.
- The surfaces were assumed isothermal and gray, that is, as emitting and reflecting diffusely.
- The considered surfaces were assumed to form an insulated system, that is, without radiative heat transfer to the environment.

The radiation thermometer measures the target exitent radiance L_{ex}. (In our case, the system supplies a signal related to temperature in converting to radiance with Planck's law.) In our description of the model, radiance is used instead of radiant power for convenience, since they are simply related as $P_{ex_i} = A_i \cdot L_{ex_i}$. However, the measured radiance includes the term L_{em}, due to target temperature, and the term L_r, from the reflection on the target surface of the radiances exitent from other bodies, since we are dealing with nonideal bodies. This yields

$$L_{ex_i} = L_{em_i} + L_{r_i} = L_{b_i} \cdot \epsilon_{m_i} + L_{r_i} \tag{1}$$

The earlier model uses an $(n \times n)$ system, with n representing the number of modeling surfaces, to calculate the L_{ex_i} exiting the surfaces, and thus assuming a given temperature distribution, L_b. By contrast, the proposed model envisages direct measurement of the surface-exitent radiances with a 360-deg scan. Having determined the L_{ex_i} of all the surfaces, except top and bottom (whose calculation assumptions will be detailed in the section dealing with the angle factor calculation), we can compute the corresponding reflected radiances for each surface, since

$$L_{r_i} = \frac{(1 - \epsilon_{m_i})}{A_i} \cdot \sum_{J=1}^{n} A_j L_{ex_j} F_{ij} \tag{2}$$

where F_{ij} is the ratio between the power ($P_{ex_{ij}}$) exitent from the jth surface reaching the ith surface and the total power (P_{ex_i}) exitent from the ith surface

$$F_{ij} = \frac{P_{ex_{ij}}}{P_{ex_i}} \tag{3}$$

Combining Eqs. (1) and (2), we get

$$L_{b_i} = \frac{1}{\epsilon_{m_i}} \left[L_{ex_i} - \frac{(1 - \epsilon_{m_i})}{A_i} \cdot \sum_{J=1}^{n} A_j L_{ex_j} F_{ij} \right] \tag{4}$$

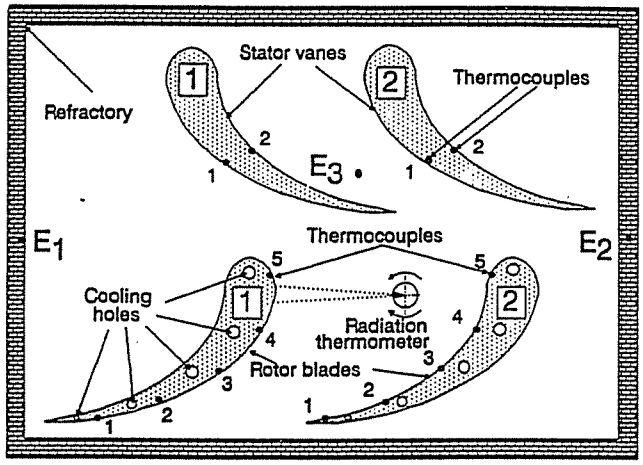

Fig. 1 Experimental setup

Thus, having determined the radiance of black body L_{b_i} we can obtain the classical form of Planck's law to determine T_i by finding the apparent value of the emissivity ϵ_{a_i} of the ith element of the surfaces considered. Applying the analytical definition (Ono, 1988)

$$\epsilon_{a_i} = \frac{L_{ex_i}}{L_{b_i}} \tag{5}$$

we obtain an inverted Planck's law

$$T_i = \frac{c_2}{\lambda \cdot \ln\left(1 + \dfrac{c_1 \epsilon_{a_i}}{\lambda^5 L_{ex_i}}\right)} \tag{6}$$

We can thus determine the correct temperature of all the isotherm surfaces used in modeling the geometry, taking into account the reflected radiation term, since electromagnetic radiations are always present in gas turbines: With heat flowing only from the higher to the lower-temperature body, the electromagnetic waves, in this case infrared, emitted through the body's heat radiation, reach all the other optically accessible bodies without being affected by their temperature. Therefore, having reached the real body surface, the electromagnetic radiations reflect only in relation to the material properties, i.e., wholly independently of body temperature. Evidently, all the radiation thermometer readings are diversely affected by this value, which, if disregarded, produces an incorrect temperature evaluation.

Experimental Model

The static model used in experimental testing is schematically illustrated in Fig. 1. Like the earlier version (De Lucia

Nomenclature

A = surface area, m^2
a = distance, m
c_1 = first radiation constant, $W\ \mu m^4 m^{-2}\ sr^{-1}$
c_2 = second radiation constant, $\mu m\ K$
F = angle factor
h = height, m
L = radiance, $W\ m^{-2}\ sr^{-1}$
l = length, m
n = number of surfaces per side (simplified geometry)
P = radiant power, W
r = distance between surfaces, m
s = width, m
T = temperature, K
x = spatial coordinate, m
α = angle between target and surface (Figs. 3 and 4)
γ = angle between perpendicular and y axis, rad
ϵ = emissivity
λ = wavelength, μm
φ = angular width, rad

Subscripts

a = apparent
b = black-body conditions
em = emittent
ex = exitent
i, j = ith and jth elements
m = material
r = reflected

and Lanfranchi, 1994), it is composed of two stator vanes and two rotor blades instrumented with K-type thermocouples (precision: 0.4–0.7 percent) simulating a 10 MW heavy-duty gas turbine. The model has been redesigned for displacement capabilities and with optimized cooling and radiation thermometer-positioning systems.

The blades and the vanes were of completely oxidized inconel with an emissivity of 0.83. The static model was lined in a refractory material with an emissivity of 0.3. We assumed that these values were constant in our working temperature range of 650–950°C. The silicon photodiode used in the radiation thermometer probe detects 1 μm wavelength radiances with a very narrow bandwidth to reduce negative effects that would have otherwise been produced.

The position of the radiation thermometer in our experimental setup, which is evidently impossible in an operating turbine, was selected solely to facilitate the construction of the experimental setup and to provide an optimum viewing angle (delimited by the perpendicular to the surface midpoints and the radiation thermometer viewing line) with respect to our area of interest (primary zone). In the operating turbine, however, the same optimum viewing angle can be attained from a different position. This is achieved by exploiting the motion of the moving blades when the relationship between the blade rotating and sampling frequencies is known, since, in gas turbine geometry, the radiation thermometer is far more sensitive to the viewing angle than the target surface distance.

The development of a more sophisticated experimental model requires the use of a larger number of complex devices. In the experimental setup, the radiation thermometer probe is housed inside a viewing tube (optional in standard applications where the sensor is preferably tilted at a preset angle; Kirby et al., 1986). At one end of the radiation thermometer viewing tube is a rhodium–platinum mirror with a 45-deg inclination that deviates the radiation by 90 deg. This provides a 360-deg scan by simple rotation of the viewing tube, while the rest of the system remains immobile.

However, in addition to representing an added expense, the mirror obviously introduces a potential source of additional noise in the measuring chain. To counter the effects of the mirror's high degradability index due to the turbine environment, which indicates reduced reflectivity, it is necessary to incorporate an effective cooling system. We selected nitrogen gas as a coolant and also to clean the mirror surface. In addition, the use of the mirror calls for special care in the angular calibration of the radiation thermometer (angular calibration being necessary in view of the fact that the measured signal is related to the angle at which the surface is viewed). It is thus possible to interpret the data measured during the 360-deg scan properly and evaluate the radiances coming from the surfaces at several different viewing angles. Lastly, a computerized radiation thermometer displacement system permits scanning via a law of motion that allows the data to be acquired and correlated to the relative geometric surface used in discretizing the system.

The experimental setup is wholly computerized. Among the required inputs are furnace temperature (in our experimental case) or operating conditions such as delivered power or reference temperature (in the case of operating machines). Decisions regarding whether or not to conduct update scans of the reciprocal radiances for calculating the target temperature are based on the changes in conditions indicated by the inputs. However, owing to the low sensitivity of the system (De Lucia and Lanfranchi, 1994), frequent updates are unnecessary. In addition, the higher the number of discretization surfaces, the lesser the system sensitivity to temperature variations.

Testing was carried out at steady-state condition at furnace temperatures ranging from 650°C to 950°C. The blade

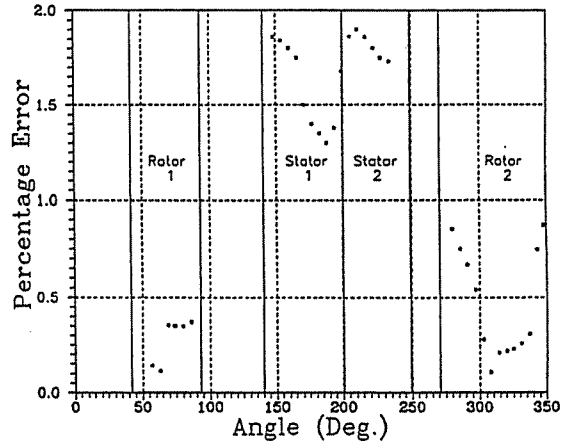

Fig. 2 Experimental results in terms of temperature error

cooling loop relative pressures were varied between 0–2 bar, thereby creating a blade-furnace temperature difference ranging from 0°C to 200°C and blade-to-blade temperature difference ranging from 0°C to 100°C. The nitrogen flow in the pneumatic loop was regulated on the basis of indications from thermocouples positioned by the lens and the nitrogen exiting the viewing tube. A vacuum pump connected to a duct coaxial to the viewing tube was used to remove the incoming nitrogen, thereby preventing leakage of cold gas that could cause uncontrolled blading and system temperature fluctuations at steady-state condition.

In comparison to the earlier model, which only corrects target temperature, the enhanced model has the advantage of furnishing a global description of the temperature distribution over the scanning plane surfaces without necessitating solution of a linear equation system and without requiring information on the theoretical temperature distribution. In addition, by moving the radiation thermometer radially with respect to the machine or vertically as in the experimental model, we obtain a complete mapping of the hub-to-tip blading temperature.

Test Results

The curve in Fig. 2 represents the percentage difference between the model-processed temperature and the actual temperature measured by the thermocouples positioned as in Fig. 1. Test temperatures were 800°C for the furnace, 670°C for blade 1, 720°C for blade 2, and 780°C for the two stator vanes. The positioning system for the 360-deg scan acts on the radiation thermometer viewing tube with a step-by-step rotation of 4–5 deg gradients to provide a slight overlap between successive positions so that no surface radiance data are missed.

Since the errors for blades 1 and 2 are comparable to the thermocouple errors, we can infer that the model worked without error in the primary zone, which, in our case, was the rotor blades. Generally, the error is primarily a result of two factors: (1) the error in the angular calibration, which, however, is necessary to account for the steep surface-view line inclination (to facilitate use of the technique by operators without special training, the angular calibration has not been fully considered herein) and (2) the glare from the furnace's background refractory surface. Since the law of motion does not account for the change from the blade to the refractory surface, measurements on the steeply inclined blading edges are inevitably affected by radiations from the refractory surface.

The error is analogous for the points relative to the stator vanes, reaching almost 2 percent with the radiation thermometer positioned for maximum accuracy in the primary

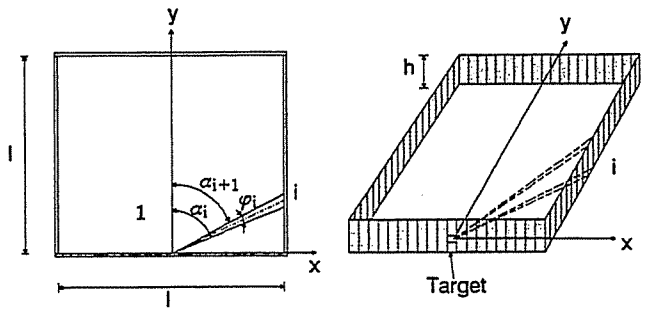

Fig. 3 Simplified geometry

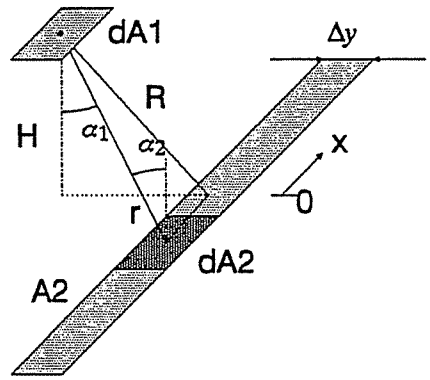

Fig. 4 Model A geometry

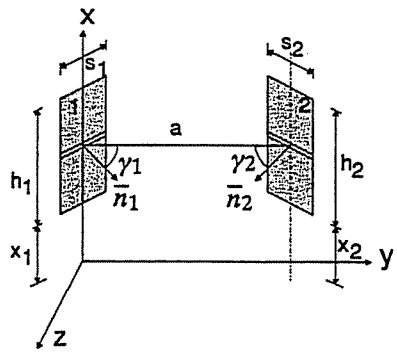

Fig. 5 Model B geometry

measuring zone, in this case the rotor blades, to the disadvantage of the other surfaces. In other words, the vane surfaces view the radiation thermometer at a considerable angle, thereby mandating correct angular calibration. Unfortunately, the vanes being stationary, the position of the radiation thermometer must be optimized in relation to the investigation zone. As validated by the experimental results, system optimization is not normally necessary—however, when optimization is required, a high level of detailed information is necessary, which might be unavailable. However, the aim of this work was simply to validate the reliability of the model for use by operators without specific training. We wanted to avoid having to overly refine the hardware and/or management systems, since, having obtained satisfactory results, focusing on error reduction at this stage rather than during the application of the system to the actual turbine would have represented a considerable waste of effort.

The test results revealed an appreciable sensitivity of the method to the angle factors. As a result, we decided to investigate the parameters affecting the accuracy of the angle factor calculation.

Considerations Concerning the Angle Factors

The method is extremely sensitive to the angle factor calculation, with slight variations amplifying the temperature error due to the six- to ninefold difference in magnitude between the angle factor and L_{ex} in the reflected radiance calculation [Eq. (2)]. Hence, measuring accuracy is closely related to proper evaluation of the angle factors and thus to the system's geometric discretization. Having completed the discretization, we can then assign a given weight to the isothermal areas through the angle factors. Hence, even a tiny error at this stage can notably affect the final temperature calculation in relation to the surface area's absolute temperature during operation. To this end, we shall present some calculations for a simple geometry to highlight the parameters affecting accuracy and to what degree they do so.

The simplified geometry represented in Fig. 3 is composed of a closed box of fixed length l and variable height h. By varying the n number of surfaces used in modeling the sides, we can reproduce the typical decision situations presented to the operator when deciding how the gas turbine geometry should be discretized (Douglas, 1980).

Angle factor calculations are based on the general definition in Eq. (7) (Sparrow and Cess, 1978)

$$F_{ij} = \frac{1}{A_i}\int_{A_i}\int_{A_j} \frac{\cos \Phi_i \cos \Phi_j}{\pi r^2} dA_i dA_j \qquad (7)$$

The literature provides several integrated formulas for calculating angle factors for elementary known geometries with appropriate approximations (Bejan, 1993; De Lucia and Lanfranchi, 1994; Kreith, 1973; Sparrow and Cess, 1978). The two most promising solutions were examined: the model proposed by Bejan (1993) hereinafter designated model A, which was adapted and implemented to account for the finite dimensions and the top and bottom surfaces, and the model proposed by De Lucia and Lanfranchi (1994), hereinafter designated model B.

Referring to Figs. 3 and 4, Bejan's formula for two thin, facing-plane, isothermal surfaces integrated between $-h/2$ and $h/2$ is

$$F_{1,2} = \frac{1}{\pi}(\sin \alpha_{i+1} - \sin \alpha_i) \cdot \left[\tan^{-1}\left(\frac{h}{2r}\right) + 2 \cdot \frac{h \cdot r}{4r^2 + h^2}\right] \qquad (8)$$

By contrast, De Lucia and Lanfranchi's general formula referring to two planar surfaces positioned as in Fig. 5 is

$$F_{1,2} = \frac{s_1 s_2 \cos \gamma_1 \cos \gamma_2}{2\pi A a} \cdot \left[(x_1 + h_1 - x_2) \cdot \tan^{-1}\left(\frac{x_1 + h_1 - x_2}{a}\right) + (x_1 - h_2 - x_2) \cdot \tan^{-1}\left(\frac{x_1 - h_2 - x_2}{a}\right) - (x_1 - x_2) \cdot \tan^{-1}\left(\frac{x_1 - x_2}{a}\right) - (x_1 + h_1 - x_2 - h_2) \cdot \tan^{-1}\left(\frac{x_1 + h_1 - x_2 - h_2}{a}\right)\right] \qquad (9)$$

which, in the simplified geometry, reduces to

$$F_{1,2} = \frac{s_1 s_2 \cos \gamma_1 \cos \gamma_2}{\pi A a} \cdot \left[h \cdot \tan^{-1}\left(\frac{h}{a}\right)\right] \qquad (9a)$$

To account for the top and bottom edges, we used (De Lucia and Lanfranchi, 1994)

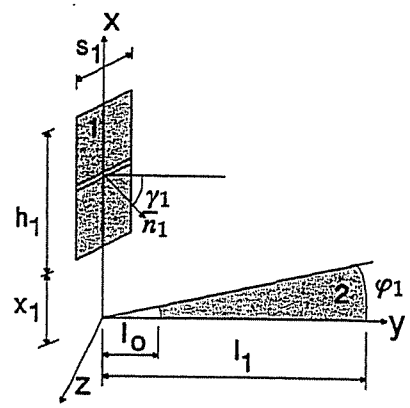

Fig. 6 Common geometry

$$F = \frac{s_1}{2\pi A}[\sin(\gamma_1 + \varphi_1) - \sin(\gamma_1)] \cdot \left[x_1 \tan^{-1}\left(\frac{l_0}{x_1}\right) - x_1 \tan^{-1}\left(\frac{l_1}{x_1}\right) - (x_1 + h_1) \cdot \tan^{-1}\left(\frac{l_0}{x_1 + h_1}\right) + (x_1 + h_1) \cdot \tan^{-1}\left(\frac{l_1}{x_1 + h_1}\right)\right] \quad (10)$$

which, in the simplified geometry (Fig. 6), becomes

$$F = \frac{s_1}{2\pi A}[\sin(\gamma_1 + \varphi_1) - \sin(\gamma_1)] \cdot \left[h \cdot \tan^{-1}\left(\frac{l_1}{h}\right)\right] \quad (10a)$$

The experimental model does not allow measurement of the radiances exiting the circular sectors of the top and bottom surfaces, since mirror displacement would necessitate an additional degree of freedom, thereby complicating the modeling procedure. Hence, for lack of more precise information, by assigning the same temperatures to the circular sectors previously measured for the correspondent rectangular thin strip, we can reduce error to approaching zero for large-size machines, i.e., those with high h/l ratios.

The main parameters to be defined for discretizing the geometry and thus calculating the angle factors are:

1 The number of plane surfaces n for approximating the blade profiles.
2 The geometry's h/l ratio.

Since l is a characteristic geometric parameter of gas turbines, we can divide h into several parts. Note that h can be the total blade height or only a part of blade height, in which case it is necessary to conduct the calculation by circular rows. The h/l parameter varies from 0.3 to 5.5 for typical heavy-duty gas turbine geometries.

To allow for examination of a suitable number of situations, the simplified geometry was nondimensionalized assuming side l of unitary length and varying the number of surfaces n by which each side is discretized, with h constant (which modifies the h/s ratio), and then varying h at n constant. The results, given in percentage of error, refer to one (since the summation of all the angle factors for a well-discretized closed geometry should be unitary), thereby showing the relation of the error as a function of the variations in the parameters.

With model A (Fig. 7), as h/l varies, there is a maximum around 2.5 where the system loses accuracy and shows poor sensitivity as n varies. However, even with n variable between 5 and 20, the improvement is only 0.8 percent of the value, with the curves overlapping between 20 and 100, while, if h/l is varied from 0.1 to 6, the error increases by one magnitude. By contrast, model B (Fig. 8) markedly improves

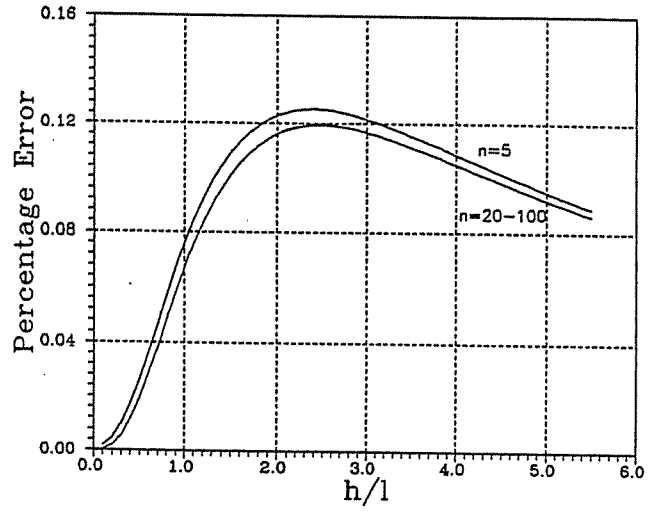

Fig. 7 Angle factor error (model A)

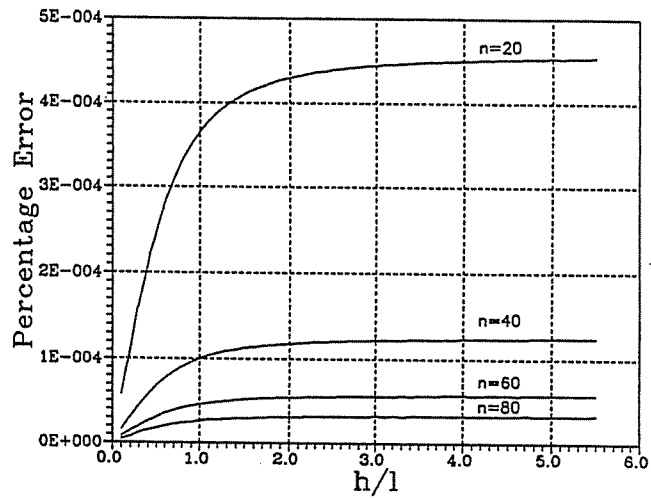

Fig. 8 Angle factor error (model B)

when n is increased and loses sensitivity to h/l at values in excess of 2. The advantages to be gained from increasing the discretization surface are evident (improved accuracy of around two to three orders of magnitude), since the curves do not overlap as in the previous case.

In both cases, with $h/l < 2.5$, the error decreases as h/l decreases. While, with geometric conditions being equal, we can reduce h/l by repeating the calculation for different circular rows, this notably increases complexity and, in addition, since the two models were developed for thin-strip isothermal surfaces, an excessive decrease could create problems in the h/s parameter, and thus negatively affect accuracy. To be able to assume isothermal thin strips for the surface discretization, we must necessarily consider the h/l ratios in relation to the actual machine geometric conditions such as swirl and, in addition, to the radial temperature distributions. With appropriate geometric conditions and radial temperature distribution, model B allows performing a sole angle factor calculation without resorting to circular rows.

Model A, while simpler, is more than two orders of magnitude less accurate than model B. Further, model A is exceedingly sensitive to the h/l ratio, whereas model B is affected primarily by n for h/l values above 2. Hence, model A should be used when it is not possible or convenient to increase n, while model B should be used in all other cases for accuracy.

From the above, it is evident that the angle factor calculation is more complex than the radiation thermometer measurements—albeit with the advantage of not having to be repeated unless the machine geometry is changed. Hence, the procedure can be carried out by two different operators: one without special training to carry out the measurements and the other with the requisite mathematical skills to calculate the angle factors. This means that, once the latter are calculated, the turbine manufacturer can then furnish the angle factors without having to divulge proprietary information regarding machine geometry.

Conclusions

- The scanning radiation thermometry technique described requires no prior knowledge of theoretical gas turbine temperature distribution and, in addition, does not require specially trained operators.
- The angle factors, calculated by personnel possessing the requisite mathematical skills, can be furnished by the manufacturer in lieu of proprietary information about machine geometry.
- The model furnishes the steady-state and near-steady-state temperature distribution with an error comparable to that of the measuring chain in the primary measuring zone.
- Error can be further reduced, especially in the vanes, by refining the model in terms of angular calibration, positioning the radiation thermometer with respect to the vanes, and optimizing the law of motion.
- The model furnishes not only target temperatures, and thus the distribution of the temperatures obtained from the blade movements, but also, without further complicating the calculation, a 360-deg distribution.
- In the experimental testing, as the model was found to be sensitive to the angle factors and thus to parameter discretization, two angle factor calculation methods were examined: The simpler one proved useful when it is not possible or convenient to increase n, while the more complex one is recommended in all other cases for accuracy.

Acknowledgments

The authors are grateful to Pierluigi Nava and Valter Quercioli of NuovoPignone and Umberto Lucia for their valuable technical contribution and to Professor Ennio Carnevale for his unfailing support. The support of NuovoPignone S.p.A. is also gratefully acknowledged.

References

Bejan, A., 1993, *Heat Transfer*, Wiley, New York.

Beynon, T. G. R., 1981, "Turbine Pyrometry—An Equipment Manufacturer's Viewpoint," ASME Paper No. 81-GT-136.

Beynon, T. G. R., 1982, "Infrared Radiation Thermometry Applied to the Development and Control of Gas Turbine Engines," *Proceedings, International Conference on Infrared Technology*, Butterworth Scientific Ltd., Sevenoaks, United Kingdom, pp. 3–16.

De Lucia, M., and Lanfranchi, C., 1994, "An Infrared Pyrometry System for Monitoring Gas Turbine Blades: Development of a Computer Model and Experimental Results," ASME JOURNAL OF ENGINEERING FOR GAS TURBINES AND POWER, Vol. 116, pp. 172–177.

DeWitt, P. D., and Incropera, F. P., 1988, "Physics of Thermal Radiation," *Theory and Practice of Radiation Thermometry*, P. D. DeWitt and G. Nutter, eds., Wiley, New York, pp. 21–89.

Douglas, J., 1980, "High-Speed Turbine Pyrometry in Extreme Environments," *Proceedings, New Orleans Gas Turbine Conference*, ASME, New York, pp. 335–343.

Kirby, P. J., Zachary, R. E., and Ruiz, F., 1986, "Infrared Thermometry for Control and Monitoring of Industrial Gas Turbines," ASME Paper No. 86-GT-267.

Kreith, F., 1973, *Principles of Heat Transfer*, Dun-Donnelley Publishing Corporation, New York, pp. 217–304.

Love, T. J., 1988, "Environmental Effects on Radiation Thermometry," *Theory and Practice of Radiation Thermometry*, P. D. DeWitt and G. Nutter, eds., Wiley, New York, pp. 189–229.

Ono, A., 1988, "Methods for Reducing Emissivity Effects," *Theory and Practice of Radiation Thermometry*, P. D. DeWitt and G. Nutter, eds., Wiley, New York, pp. 565–623.

Schulemberg, T., and Bals, H., 1987, "Blade Temperature Measurements of Model V84.2 100 MW/60 Hz Gas Turbine," ASME Paper No. 87-GT-135.

Scotto, M. J., and Eismeier, M. E., 1980, "High-Speed Noncontacting Instrumentation for Jet Engine Testing," ASME JOURNAL OF ENGINEERING FOR GAS TURBINES AND POWER, Vol. 102, pp. 912–917.

Sparrow, E. M., and Cess, R. D., 1978, *Radiation Heat Transfer*, Hemisphere Publishing, Washington, DC, pp. 81–143.